PFC/JA-89-2

Electron Cyclotron Wave Propagation and Absorption in the Compact Ignition Tokamak

R. C. Myer and M. Porkolab

Plasma Fusion Center
Massachusetts Institute of Technology
Cambridge, MA 02139

G. R. Smith

Lawrence Livermore National Laboratory
Livermore, CA 94550

A. H. Kritz

Hunter College, CUNY,
New York, NY 10021

June 1989

Electron Cyclotron Wave Propagation and Absorption
in the Compact Ignition Tokamak

Richard C. Myer and Miklos Porkolab
Plasma Fusion Center, Massachusetts Institute of Technology
Cambridge, MA 02139

Gary R. Smith
Lawrence Livermore National Laboratory, University of California
Livermore, CA 94550

Arnold H. Kritz
Hunter College/CUNY, New York, NY 10021

Abstract

The possibility of heating the Compact Ignition Tokamak (CIT) with electron-cyclotron power at 280 GHz (fundamental cyclotron resonance) is examined by simple analytic estimates and by detailed computational means. Efficient single-pass absorption of the O-mode polarization is accomplished by scanning the angle of injection of the microwave power from 60° to 90° relative to the toroidal magnetic-field direction as the field intensity is ramped from 7 or 8 to 10 T and the volume-average beta increases from 0.4% to 2.8%. Efficient absorption occurs for the range of central densities from 2 to $8 \times 10^{20} m^{-3}$ and central temperatures from 5 to 20 keV. Thus, electron-cyclotron-resonance heating, using either gyrotrons or free-electron lasers, offers a reasonable heating scenario from the ohmic phase to the ignition phase even with a single-frequency RF source.

I. Introduction

The most recent operating scenario of the Compact Ignition Tokamak (CIT) calls for ramping of the toroidal magnetic field from 7.0 or 8.0 to 10.0 T in a few seconds, followed by a burn cycle and a ramp-down cycle. Simultaneously, the plasma must be heated from an initial low-beta equilibrium ($\bar{\beta} \simeq 0.44\%$ at 7.0 to 8.0 T) to a final burn equilibrium in the range of 2.5-5.0%, having 10.0 T on the magnetic axis [1]. Since the toroidal plasma current will be ramped at the same time and since the available time for flat-top magnetic field must be reserved for the burn cycle, it is imperative that densification and heating be

carried out as the magnetic field is ramped. At first it would appear that this requirement will either restrict deployment of possible RF heating techniques (ICRF, ECRH) to ones which allow continuous sweeping of the source frequency, or force one to accept an operating scenario in which the resonance is swept from the high-magnetic-field side to the low-field side as the magnetic field on axis increases. The former approach places severe demands on RF source technology (dynamically tunable sources at high power are hard to come by in either the ICRF or ECRH regime, with the possible exception of free-electron lasers (FELs)). The latter approach possibly leads to non-optimal confinement because it cannot achieve the desired heating profiles. In the case of swept frequencies, further difficulties may arise with certain elements of the transmission line (tuning elements in the case of ICRF are frequency sensitive, while windows, polarizers, etc., for ECRH may be frequency dependent).

Here we examine an alternative approach which is applicable to ECR heating, using either gyrotrons or FELs. The frequency remains constant, while the angle of injection is varied by simply rotating a reflecting mirror placed in the path of the incident microwave beam. The rotating mirror permits one to launch waves with sufficiently high $N_\parallel$ so that the Doppler broadened resonance of particles on the magnetic axis with 7.0-8.0 T can provide adequate absorption. In contrast to the heating scenarios recently proposed which rely on downshifted frequencies and finite $N_\parallel$ to ensure penetration and absorption of the extraordinary mode (X-mode, $\vec{E}_{RF} \perp \vec{B}$) polarization for frequencies below the fundamental [2], here we propose to use an upshifted frequency with finite $N_\parallel$ for the ordinary mode (O-mode, $\vec{E}_{RF} \parallel \vec{B}$) polarization. The O-mode is accessible from the outside (low-field side) of the torus provided the density is such that $\omega_{pe} \lesssim \omega \approx \Omega_e$ (max). The advantage of heating above the fundamental cyclotron frequency initially is that as the field is ramped absorption near the center can be maintained, even when the field is at its maximum. As the resonance layer moves toward the magnetic axis the rotating mirror can sweep the beam toward perpendicular to reduce the Doppler width and avoid heating the plasma edge. At $B(0) = 10.0$ T the beam will be at normal incidence with strong absorption immediately on the high-field side of the resonance. Considering $f = 280$ GHz for a central heating at $B(0) = 10.0$ T, the maximum cut-off density is at $n_{crit} \approx 9.7 \times 10^{20} \mathrm{m}^{-3}$. We expect reasonable wave penetration and heating up to $0.9 n_{crit}$ or $n_e(0) \approx 8.7 \times 10^{20} \mathrm{m}^{-3}$ which is about the maximum central density in CIT. On account of the Murakami density limit [1], CIT is expected to operate at $\bar{n} \simeq 5 \times 10^{20} \mathrm{m}^{-3}$ at $B = 10.0$ T ($R = 2.1$ m, $a = 0.70$ m, $\kappa = 2.0$, $I_p \approx 10$ MA). At lower magnetic fields, beta and hence the density is expected to be lower and no wave penetration problems should be anticipated. In addition to its simplicity, this technique requires rotation of the beam injection angle only in the toroidal direction.

Furthermore, the propagating rays and the absorption profiles are not excessively sensitive to the angle of injection (as long as the density is not near the cut-off value).

The alternate technique proposed by the authors of Reference 2 enjoy the advantage of lower frequency (200 GHz vs. 280 GHz proposed here). However, there are several disadvantages of using lower frequencies when applied to heating compact ignition devices:

(a) Only the top-launch scenario was useful for heating while ramping the magnetic field, density and current. However in such a launching scenario, the absorption profile is very sensitive to the exact launching angle (both in the poloidal and toroidal direction, especially at higher densities). Such a control of ray trajectories may be made more difficult if we consider scattering by low frequency density fluctuations at the plasma periphery. Consequently, sawtooth activity control by precise control of the radial power deposition profile may be difficult.

(b) Lack of easy access to the top (bottom) of the vacuum chamber in the presence of divertors is a serious drawback of such a technique, especially if one has to install, and maintain reflecting mirrors in a burning plasma environment. Further difficulties may arise if one considers moving parts with two degrees of freedom.

(c) There is the potential of RF breakdown in the beam-line (path) where the $\omega = \omega_{ce}$ resonance surface is crossed, which is inherent in the low frequency scenario.

We note that recent advances in source technology (gyrotrons and FELs) make ECR heating of CIT at 280 GHz a viable option. Furthermore, ECRH is also attractive from the point of high-power-density transmission (Power/Area $\gtrsim$ 100 MW/m^2 so that 30 MW of ECR power may be transmitted through two CIT ports with dimensions of 0.40 $\times$ 1.0 m each). Quasi-optical transmission techniques may be utilized at 280 GHz so that no internal antenna structure (with the exception of the rotating mirror placed in the port) is required, a definite advantage over other techniques of heating a burning plasma. Equilibration of temperature between electrons and ions (τ_{eq}) is expected to be significantly shorter than typical energy confinement times, τ_E. For example, at $n_e \approx 1.0 \times 10^{20}$m^{-3}, $T_e = 5$ keV (low-beta equilibrium), and assuming $Z_{\text{eff}} \approx 1.5$ we estimate $\tau_{eq} \approx 60$ msec, while at $n_e(0) \approx 8 \times 10^{20}$m^{-3}, $T_e \approx T_i \approx 20$ keV (high-beta equilibrium), $\tau_{eq} \approx 65$ msec, both shorter than the expected energy confinement time ($\tau_E \gtrsim 0.1$ s at low beta and $\tau_E \gtrsim 0.5$ s at high beta).

II. Wave Propagation and Absorption Physics

An estimate of single-pass absorption of rays in the Doppler regime passing through the resonance layer near the plasma center can be obtained from the well known formula [3, 4] for O-mode absorption. Taking $A = 1 - \exp(-\Gamma)$, where A is the absorption per pass, the optical depth is

$$\Gamma \simeq \frac{\pi}{2} R \frac{\omega}{c} \left(\frac{T_e}{m_e c^2} \right) \alpha (1 - \alpha)^{1/2}, \tag{1}$$

where $\alpha = \omega_{pe}^2/\omega^2, \omega \simeq \Omega_e$, and $N_\parallel^2 \ll 1$. For CIT parameters we obtain $\Gamma \simeq 140$ for $T_e \gtrsim 10$ keV, $\alpha \simeq 0.8$ ($n \sim 8 \times 10^{20} \mathrm{m}^{-3}$), which corresponds to very strong absorption and is likely to cause strong non-central absorption. Hence, in this case we recommend making use of the relativistic absorption regime, namely we consider near perpendicular wave propagation, $N_\parallel < (T_e/m_e c^2)^{1/2}$. The relativistic resonance condition,

$$\omega - \frac{\Omega_e}{\gamma} - k_\parallel v_\parallel = 0, \tag{2}$$

predicts that there are no resonant particles on the low-magnetic-field side ($\omega > \Omega_e(r)$) for near perpendicular injection ($N_\parallel \to 0$). Once the wave passes through the cyclotron resonance layer, absorption is expected to be complete in a very short distance. The absorption may be estimated from the relativistic formula given by Bornatici, et al. and references therein [4] for strong absorption

$$\mathrm{Im}(N_\perp) = \frac{1}{2^{3/2}} \left(1 - \frac{\omega_p^2}{\Omega_e^2} \right)^{1/2} \left(\frac{\omega_p^2}{\Omega_e^2} \right) \frac{[-F_{7/2}''(z_1)]}{|G_{7/2}|(G_{7/2}' + |G_{7/2}|)^{1/2}} , \tag{3}$$

where

$$G_{7/2} = G_{7/2}' + i G_{7/2}'' = 1 + \frac{1}{2} \frac{\omega_p^2}{\Omega_e^2} F_{7/2}(z_1),$$

$$z_1 = \frac{(\omega - \Omega_e)}{\omega} \frac{m_e c^2}{T_e},$$

and $F_{7/2} = F_{7/2}' + i F_{7/2}''$, is the relativistic form of the plasma dispersion function

$$F_q(z) = -i \int\limits_0^\infty \frac{d\tau \, \exp(iz\tau)}{(1 - i\tau)^q}, \quad \mathrm{Im}(z) > 0. \tag{4}$$

Prime and double prime quantities refer to the real and imaginary parts, respectively. For example, for $T_e = 10$ keV, we get maximum damping at $\Delta r \simeq 10$ cm away from

4

resonance (on the high-field side) where $z_1 \simeq -2.5$ and $\text{Im}(k_\perp) \simeq 2.8 cm^{-1}$ for $\omega_p^2/\Omega_e^2 = 0.8$. Therefore, most of the power is absorbed between the center and $\Delta r \approx 10$ cm on the high-field side. Similar results are obtained at $T_e = 20$ keV for $\Delta r \simeq 5$ cm, where complete absorption takes place in a few centimeters on the high-field side. Thus, even in the high-beta regime, the waves penetrate fully to the plasma center (i.e., resonance layer), where complete absorption takes place. This property of EC wave propagation can be used to localize absorption even in a burning plasma if central heating is desirable. If subsequently we wish to stabilize sawteeth ($q = 1$ surface) or if we wish to stabilize $m = 2$ modes ($q = 2$ surface) and thus avoid disruption, we may have to change the angle of injection during the burn phase, at least for part of the RF power. The result would be non-central, off-axis heating, leading to control of MHD activities. An alternate scenario for MHD control would call for lowering the frequency while retaining normal incidence (a possibility for FEL type sources).

In order to employ a single frequency as the magnetic field is ramped, we propose to use the Doppler regime for $\omega > \Omega_e$ (non-resonant case, $7 \lesssim B(T) < 10$), and relatively low β. The importance of cyclotron absorption in the Doppler regime for the non-resonant case can readily be estimated. The spatial decrement for the O-mode propagation in the Doppler regime can be deduced from [3,4]. In particular, for $\omega \neq \Omega_e$, $\zeta_e^2 = (\omega - \Omega_e)^2/k_\parallel^2 v_{te}^2 \gg 1$ Eq. 3.1.67 in Ref. 4 reduces to the result of Ref. 3, namely

$$2\,\text{Im}(k_\perp) = \left(\frac{\pi}{2}\right)^{1/2} \frac{\omega}{c} \left(\frac{N_\perp}{N_\parallel}\right) \left(\frac{\omega_{pe}^2}{\Omega_e^2}\right) \left(\frac{T_e}{m_e c^2}\right)^{1/2} \zeta^2 \exp(-\zeta^2), \qquad (5)$$

where $v_{te} = (2T_e/m_e)^{1/2}$. Here $N_\perp$ and $N_\parallel$ are the components of the index of refraction perpendicular and parallel to the magnetic field, respectively. We note that the absorption is controlled by the exponential factor. Assuming that $\omega > \Omega_e$ everywhere in the plasma, and that absorption occurs within a radial distance of $\Delta r \lesssim 0.5a$, where a is the minor radius, for $a \simeq 70$ cm, $f = 280$ GHz, $\omega_{pe}^2/\Omega_e^2 \simeq 0.4$ (i.e. $B = 7$ T, $n_e \simeq 2 \times 10^{20} \text{m}^{-3}$), $T_e \simeq 10$ keV, $N_\perp/N_\parallel \simeq 1$, the condition for significant single-pass absorption, $2\,\text{Im}(k_\perp)\Delta r \simeq 1$, is obtained for $\zeta^2 - \ell n\zeta^2 \simeq 4.6$ or $\zeta \simeq 2.55$. We take into account the toroidal effect that $N_\parallel$ increases as $N_\parallel(R) \propto 1/R$, where R is the major radius, as the wave penetrates to the center and beyond. Then for $a/R \simeq 1/3$, $N_\parallel(a) \simeq 0.50$ ($30°$ launch angle at the plasma edge), $N_\parallel(R) \gtrsim 0.67$ for $r \lesssim 0$, and $\zeta = 2.55$ yields $B = 7.5$ T for the above parameters, so that $\omega/\Omega_e \simeq 1.32$. We note that on the high-magnetic-field side beyond the plasma center, $N_\parallel$ further increases and ω/Ω_e decreases, hence absorption will rapidly increase for reasonable temperature profiles. Thus, effective wave absorption can be achieved even for an isotropic Maxwellian distribution function. Although here we ignored relativistic

5

effects, it is clear from the resonance condition Eq. (2), and from more accurate theoretical treatments [5, 6, 7] that the main consequence of retaining relativistic effects is to shift the location of absorption partially back toward the cyclotron resonance layer. We expect that quasi-linear enhanced tails would further improve single-pass absorption. These analytical estimates are verified by more exact numerical ray-tracing results presented in the next section. We shall find that for electron temperatures $T_e \gtrsim 5$ keV and magnetic fields $B(0) \gtrsim 7.0$ T, efficient single-pass absorption occurs for an incident frequency of 280 GHz, and for $B(0) \gtrsim 7.5$ T nearly complete single-pass absorption results for incident angles of $30°$ (or less) relative to the normal to $\vec{B}$.

III. Code Results

Here we study single-pass absorption of waves in equilibria representative of the CIT plasma. The plasma flux surfaces were generated by an equilibrium code [8] which used the current waveforms in the PF coil system obtained from a run of the Tokamak Simulation Code [9] with a swept divertor. The weakly relativistic ray-tracing and absorption calculations were performed using the TORCH code, developed by two of the authors (GRS and AHK), described in the Appendix. The profiles assumed for this study are square root of parabolic for the density and parabolic for the temperature. Specifically, we used $p_1 = p_3 = p_4 = 1$ and $p_2 = 0.5$ for the parameters described in the Appendix.

We first present the results of ray-tracing calculations for the non-resonant magnetic fields of $B(0) = 7.5$ T and 8.5 T in the Doppler regime. In the case of an ohmic target plasma with $B(0) = 7.5$ T, the relevant "startup" regime would be at $n_e(0) \simeq 2.5 \times 10^{20} \mathrm{m}^{-3}$ and $T_e(0) \simeq 5.0$ keV. In Figs. 1(a-c) we show cases of wave penetration and absorption for $B = 7.5$ T, $\theta = 30°$, $T_e(0) = 5$, 10, and 20 keV, keeping the density fixed at $2.5 \times 10^{20} \mathrm{m}^{-3}$. The dashed curve indicates the location of the fundamental electron cyclotron resonance layer. Figure 1 shows a projection onto the poloidal plane, while Fig. 2 shows the projection onto the equatorial plane. The solid circles shown in these figures represent the locations where the power in each ray has decreased by 20%. The absorption calculations indicate that even for the lowest temperature "startup" conditions 100% single-pass absorption is achieved. When $B(0) = 7.5$ T the resonance layer is roughly 40 cm from the magnetic axis and the absorption is significantly off-axis. As the temperature increases the damping length decreases and the absorption profile moves in toward the magnetic axis. Figures 3(a-c) show the wave penetration and absorption for $B = 8.5$ T, $\theta = 30°$, $T_e(0) = 5$, 10, and 20 keV, keeping the density fixed at $3.2 \times 10^{20} \mathrm{m}^{-3}$. Here the closer proximity of the resonance layer results in strong central heating on the magnetic axis at $T_e(0) = 5$ keV and

off-axis heating as the temperature is increased. These results can be shown more clearly by plotting the power absorption as a function of the normalized flux variable. Figures 4 and 5 show the power absorption profiles (with temperature as a parameter) corresponding to the 7.5 T and 8.5 T cases, respectively. The locations of the q=1 and q=2 surfaces are shown on the horizontal axis. We emphasize that relativistic effects are included in these calculations even in the Doppler regime. We have verified that shutting off relativistic effects shifts the absorption layer outward, toward the low field side, as expected from theory. However, the "effectiveness" of absorption is not altered in any significant way.

Since the width of the particle resonance in the Doppler regime is directly proportional to $N_{\parallel}$, the power-deposition profile is most easily controlled by changing the incident wave propagation angle θ. Figure 6 shows how the power deposition profile changes as the angle θ, measured with respect to perpendicular incidence, varies from 30° to 10° for the 7.5 T case with T_e=5 keV. The optimum angle for central heating for the 7.5 T case is approximately 30°. The power deposition profiles for 8.5 T on axis and T_e=10 keV are shown in Fig. 7. Here the optimum angle for central heating is roughly 20°. In order to keep the absorption close to the magnetic axis as the beta and magnetic field are increasing during the ramp-up, it is clear that the angle of incidence must be swept toward normal incidence to $\vec{B}$. Again, relativistic effects were included in these computations.

To avoid absorption on the low-field side and achieve wave penetration to the center at full field and beta it is necessary to operate in the "relativistic" regime ($N_{\parallel} < (T_e/m_e c^2)^{1/2}$). To evaluate absorption in such a case, we let $N_{\parallel} \to 0$ in the TORCH code. The same results were also obtained in a separate set of calculations by evaluating Bornatici's formula [Eq. (3)] along the ray trajectories generated by TORCH. Typical results are shown in Fig. 8. As we see, even in a high-beta plasma, central wave penetration is possible. Beyond the cyclotron resonance layer, complete wave absorption occurs in a radial distance of a few centimeters. We are therefore confident that these waves can penetrate to the core of even a burning plasma ($n_e(0) \simeq 8 \times 10^{20} m^{-3}, T_e(0) \sim 20$ keV), and be absorbed near the center. Similar results are obtained in the low-beta case for $T_e(0)$=20 keV, $B(0) = 10$ T. Second-harmonic resonance near the edge in the burning-plasma case absorbed at most 8% of the incident power, while in the low-beta case it amounted to less than 2% per pass. Thus, harmonic competition in CIT-like plasmas is not an issue.

As shown in Figs. 9(a–c) if the angle of injection is too large as the field increases to 10.0 T on axis we find strong off-axis absorption with the relativistic TORCH code. While strong off-axis absorption may be appropriate in a burning plasma for controlling MHD activity, in the low-beta regime central heating may be preferable to increase the density and beta.

7

Finally, we consider the efficiency of coupling to the O-mode at the edge of the plasma for a linearly polarized incident wave field whose electric field lies in the x-z plane where z is the direction of the toroidal field, and x is the radial direction. To do this we calculate the ratio of the power in the O-mode (P_O) to the total power launched (P_T) for a wave polarized such that $E_y = E_{y|O} + E_{y|X} = 0$:

$$\frac{P_O}{P_T} = \frac{|E_{x|O}|^2 + |E_{y|O}|^2 + |E_{z|O}|^2}{|E_{x|O} + E_{x|X}|^2 + |E_{z|O} + E_{z|X}|^2} \quad , \tag{6a}$$

$$= \frac{a^2 + 1 + c^2 a^2}{|1 - abc|^2 + |a - dac|^2} \quad , \tag{6b}$$

where the ratio of the field components for the X and O mode are defined as follows: $a = E_{x|O}/E_{z|O}$, $b = E_{z|X}/E_{y|X}$, $c = E_{y|O}/E_{z|O}$, and $d = E_{x|X}/E_{y|X}$. These quantities are obtained from the cold-plasma field equations, namely

$$\frac{iE_x}{E_y} = \frac{n^2 - S}{D},$$

$$\frac{E_x}{E_z} = \frac{n_\perp^2 - P}{n^2 \cos\theta \sin\theta},$$

using the appropriate value of n^2 for the X and O mode. Here S, D, and P are the components of the cold-plasma dielectric tensor in Stix' notation [10]. These expressions may be evaluated for the tenuous edge plasma by expanding the dielectric elements to first order in $\alpha = \omega_{pe}^2/\omega^2$. After a considerable amount of algebra we obtain

$$\frac{P_O}{P_T} = \frac{1}{4}\left(1 + \frac{\sin^2\theta}{\eta}\right)^2 + \frac{\cos^2\theta}{\beta\eta^2}, \tag{7}$$

where $\beta = \Omega_e^2/\omega^2$ and $\eta = (\sin^4\theta + 4\cos^2\theta/\beta)^{1/2}$. Substituting $\beta = (0.7/1.33)^2 = 0.276$ and $\theta = 60°$ for the conditions at the edge (assuming an aspect ratio of 3) in the case of nonresonant heating case (7 T) we find that $P_O/P_T \approx 0.68$. Thus, approximately 68% of the power injected will couple to the O-mode at the edge of the plasma. The remaining 32% will be in the X-mode, which is cutoff for the present low-field launch scheme and will be reflected out of the plasma. We expect that this reflected power will eventually be absorbed following conversion to the O-mode by multiple reflections on the vacuum-chamber walls as has been observed in electron-cyclotron heating experiments on DIII-D [11]. As the magnetic field is increased toward B=10.0 T on axis, the fraction of O-mode launched increases. In particular, at B=10.0 T, $\theta = 0°$ and $P_O/P_T = 1.0$.

IV. Summary and Conclusions

We have examined the possibility of ECR heating in an initially ohmically heated CIT plasma as the magnetic field is ramped from 7 to 10 T while the volume averaged beta is increased from 0.4% to 2.8%. It is found that a viable heating scenario exists by using a constant frequency source, injected from the low-magnetic-field side in the O-mode polarization, if the angle of injection can be varied in the range of 0° to 30° from the normal to the magnetic field. Starting up with an initial ohmic plasma of $n_e(0) \simeq 2 \times 10^{20} \text{m}^{-3}, T_e(0) \simeq 5$ keV, and an angle of injection of 30° from the normal to the magnetic field, the plasma may be heated to ignition-like conditions ($n_e(0) \simeq 8 \times 10^{20} \text{m}^{-3}, T_e(0) \simeq T_i(0) \simeq 20$ keV) by changing the angle of injection toward 0° as the magnetic field is ramped from $B(0) \simeq 7.0$ T to 10.0 T. Using a source frequency of 280 GHz, good central heating and nearly complete single-pass absorption can be achieved at all magnetic fields for $T_e \gtrsim 7$ keV. As long as the density and electron temperature are ramped together, equilibration between electrons and ions is expected to occur within $\simeq 60$ ms, shorter than the expected energy confinement time ($\tau_E \simeq 0.2$–1 s). Under the high-beta conditions, central absorption is ensured by the relativistic wave-particle resonance condition, operative for nearly perpendicular injection. Less than 8% of the power is absorbed by harmonic competition under all conditions. If off-axis heating were desired during the burn cycle for the purposes of controlling MHD activity, rotating the angle of injection at the appropriate time in the burn phase would suffice. In the extreme case when $q = 2$ is near the plasma edge, localized heating near this layer may require utilization of a lower frequency source.

Thus, assuming that efficient RF sources can be developed on time, ECR heating appears a promising technique to satisfy the present requirements of heating CIT to ignition-like parameters. The International Thermonuclear Experimental Reactor (ITER) may also be able to utilize the Doppler-shifted scenario for heating near the magnetic axis, where $B \simeq 5$ T, with the same 200-GHz sources required for current drive.

Appendix. Description of the TORCH Code

The ray-tracing code TORCH (an acronym for TOroidal Ray-tracing, Current-drive, and Heating) has developed from the earlier codes RAYS [12] and TORAY [13]. In contrast to the earlier codes, TORCH is constructed under the Basis System [14], which provides both an efficient structure for multiple-author programs and a powerful user interface for controlling execution of the code and plotting of the results. The Basis System was begun as part of the MERTH Project [15].

9

The TORCH code is organized as several separate modules, each of which describes a different aspect of the physics treated by the program. The modules, called physics packages, that are important for the calculations in this paper are concerned with ray tracing, plasma equilibrium, and electron-cyclotron dispersion and absorption.

On a higher level, the TORCH code is separated into compiled code (e.g., the physics packages described above) and interpretted code. The latter is simply a large set of input files that are read by a powerful parser and control the setting of variables, including scanning over ranges of variables, the running of physics packages, and the plotting of results. Users can select from the set of input files to design the calculations and output appropriate to the problem at hand. The utility of interpretted code for these purposes follows from the ease with which users can modify it and test it, because there is no need to recompile and load the physics packages for every test.

The ray-tracing package initializes and integrates the ordinary differential equations that determine the trajectories of all rays. During the integration many quantities are saved for later plotting or calculations. This package also accumulates radial profiles of power absorbed and current driven.

The equilibrium package has subroutines that are called whenever information is needed about the magnetic-field vector, the electron density and temperature, and the gradients of these quantities. A model equilibrium with circular flux surfaces is described in Ref. [13], but the present paper uses another option [16], which is described here. The magnetic field is given by

$$\mathbf{B} = F(\psi)\,\nabla\phi + \nabla\phi \times \nabla\psi, \qquad (A-1)$$

where ϕ is the toroidal angle and where the flux functions $F(\psi)$ and $\psi(R,Z)$ are input to TORCH from any code that solves the Grad-Shafranov equation

$$\triangle^*\psi \equiv R^2\,\nabla \cdot \left(\frac{\nabla\psi}{R^2}\right) = -\left(\mu R^2 \frac{dP}{d\psi} + F\frac{dF}{d\psi}\right), \qquad (A-2)$$

and produces an EQDSK output file. The density profile has the form

$$\frac{n(\psi)}{\hat{n}} = \left(1 - \tilde{\psi}^{p_1}\right)^{p_2}, \qquad (A-3)$$

where

$$\tilde{\psi} = \frac{\psi - \psi_{\text{axis}}}{\psi_{\text{edge}} - \psi_{\text{axis}}}.$$

The temperature profile may have the form

$$\frac{T_e(\psi)}{\hat{T}_e} = \left(1 - \tilde{\psi}^{p_3}\right)^{p_4}, \qquad (A-4)$$

10

The TORCH code is organized as several separate modules, each of which describes a different aspect of the physics treated by the program. The modules, called physics packages, that are important for the calculations in this paper are concerned with ray tracing, plasma equilibrium, and electron-cyclotron dispersion and absorption.

On a higher level, the TORCH code is separated into compiled code (e.g., the physics packages described above) and interpretted code. The latter is simply a large set of input files that are read by a powerful parser and control the setting of variables, including scanning over ranges of variables, the running of physics packages, and the plotting of results. Users can select from the set of input files to design the calculations and output appropriate to the problem at hand. The utility of interpretted code for these purposes follows from the ease with which users can modify it and test it, because there is no need to recompile and load the physics packages for every test.

The ray-tracing package initializes and integrates the ordinary differential equations that determine the trajectories of all rays. During the integration many quantities are saved for later plotting or calculations. This package also accumulates radial profiles of power absorbed and current driven.

The equilibrium package has subroutines that are called whenever information is needed about the magnetic-field vector, the electron density and temperature, and the gradients of these quantities. A model equilibrium with circular flux surfaces is described in Ref. [13], but the present paper uses another option [16], which is described here. The magnetic field is given by

$$\mathbf{B} = F(\psi)\,\nabla\phi + \nabla\phi \times \nabla\psi, \qquad (A-1)$$

where ϕ is the toroidal angle and where the flux functions $F(\psi)$ and $\psi(R,Z)$ are input to TORCH from any code that solves the Grad-Shafranov equation

$$\triangle^*\psi \equiv R^2\,\nabla\cdot\left(\frac{\nabla\psi}{R^2}\right) = -\left(\mu R^2\frac{dP}{d\psi} + F\frac{dF}{d\psi}\right), \qquad (A-2)$$

and produces an EQDSK output file. The density profile has the form

$$\frac{n(\psi)}{\hat{n}} = \left(1 - \tilde{\psi}^{\,p_1}\right)^{p_2}, \qquad (A-3)$$

where

$$\tilde{\psi} = \frac{\psi - \psi_{\text{axis}}}{\psi_{\text{edge}} - \psi_{\text{axis}}}.$$

The temperature profile may have the form

$$\frac{T_e(\psi)}{\hat{T}_e} = \left(1 - \tilde{\psi}^{\,p_3}\right)^{p_4}, \qquad (A-4)$$

10

or may be chosen to be consistent with the plasma pressure $P(\psi)$ used in the solution of the Grad-Shafranov equation.

The electron-cyclotron package contains subroutines to perform many calculations. Some subroutines solve the dispersion relation and calculate the dielectric tensor and its determinant and derivatives. These calculations can be done within the cold-plasma [12] or the weakly-relativistic approximations [17]. Other subroutines compute the rates of cyclotron absorption or emission under the assumptions that the electron distribution is Maxwellian and the wave amplitude is small (linear absorption). Subroutines based on three different analytic calculations are useful near the fundamental resonance if the non-relativistic approximation is valid [4, 18, 19]. For resonances up to the fourth harmonic, the weakly relativistic formulation of Shkarofsky may be used [17]. This package is used exclusively in the present paper. For arbitrary harmonics, the fully relativistic formulation of Ref. [7] is available. There is also coding for nonlinear cyclotron absorption [20, 21].

The TORCH code has other capabilities, which are mentioned briefly here. The current driven by electron-cyclotron power can be calculated [22]. Mirrors of various shapes can cause specular reflection of the rays. The code can calculate approximately the spatial profile of microwave-beam power deposited on a calorimeter located outside the plasma. The radiation temperature due to electron-cyclotron emission by thermal electrons can be calculated for each ray. TORCH also contains coding to compute, for high-frequency ($\omega \gg \omega_{pe}$) waves, the change in polarization (Stokes parameters) incurred by a ray during transit across the plasma.

Acknowledgments

or may be chosen to be consistent with the plasma pressure $P(\psi)$ used in the solution of the Grad-Shafranov equation.

The electron-cyclotron package contains subroutines to perform many calculations. Some subroutines solve the dispersion relation and calculate the dielectric tensor and its determinant and derivatives. These calculations can be done within the cold-plasma [12] or the weakly-relativistic approximations [17]. Other subroutines compute the rates of cyclotron absorption or emission under the assumptions that the electron distribution is Maxwellian and the wave amplitude is small (linear absorption). Subroutines based on three different analytic calculations are useful near the fundamental resonance if the non-relativistic approximation is valid [4, 18, 19]. For resonances up to the fourth harmonic, the weakly relativistic formulation of Shkarofsky may be used [17]. This package is used exclusively in the present paper. For arbitrary harmonics, the fully relativistic formulation of Ref. [7] is available. There is also coding for nonlinear cyclotron absorption [20, 21].

The TORCH code has other capabilities, which are mentioned briefly here. The current driven by electron-cyclotron power can be calculated [22]. Mirrors of various shapes can cause specular reflection of the rays. The code can calculate approximately the spatial profile of microwave-beam power deposited on a calorimeter located outside the plasma. The radiation temperature due to electron-cyclotron emission by thermal electrons can be calculated for each ray. TORCH also contains coding to compute, for high-frequency ($\omega \gg \omega_{pe}$) waves, the change in polarization (Stokes parameters) incurred by a ray during transit across the plasma.

Acknowledgments

References

1. Parker, R., et al., paper IAEA-CN-50/J-I-1, presented at the 12th Int. Conf. on Plasma Physics and Controlled Nuclear Fusion Research, Nice, France, October 12-19, 1988.

2. Mazzucato, E., Fidone, I., and Granata, G., Phys. Fluids, **30** (1987) 3745.

3. Porkolab, M., Friedland, L., and Bernstein, I., Nucl. Fusion **21** (1981) 1643.

4. Bornatici, M., Cano, R., DeBarbieri, O., and Engelmann, F., Nucl. Fusion **23** (1983) 1153.

5. Fidone, I., Granata, G., Ramponi, G. Meyer, R.L., Phys. Fluids, **21** (1978) 645.

6. Fidone, I., Granata, Meyer, R.L., Phys. Fluids **25** (1982) 2249.

7. Batchelor, D.B., Goldfinger, R.C., and Weitzner, H., Phys. Fluids **27** (1984) 2835.

8. Pillsbury, R.D., "PF System for the CIT 2.1 m Machine," REF:MIT-PF040888, (1988).

9. Jardin, S.C., Pomphrey, N., and DeLucia, J., J. Comput. Phys. **66** (1986) 481.

10. Stix, T.H., *The Theory of Plasma Waves*, McGraw-Hill, New York, (1962).

11. Prater, R., Bull. Am. Phys. Soc. **32** (1987) 1712.

12. Batchelor, D.B., Goldfinger, R.C., and Weitzner, H., IEEE Trans. Plasma Science **PS-8** (1980) 78.

13. Kritz, A.H., Hsuan, H., Goldfinger, R.C., and Batchelor, D.B., "Ray Tracing Study of Electron-Cyclotron Heating in Toroidal Geometry," in Proc. 3rd Joint Varenna-Grenoble International Symp. on Heating in Toroidal Plasmas, (Commission of the European Communities, Brussels, 1982), Vol. II, p. 707.

14. Dubois, P.F., Motteler, Z.C., Willmann, P.A., Allsmann, R.M., Benedetti, C.M., et al., "The Basis System," Lawrence Livermore National Laboratory Report No. M-225 (1988).

15. Nevins, W.M., Boghosian, B.M., Cohen, R.H., Cummins, W.F., Dubois, P.F., et al., in Plasma Physics and Controlled Nuclear Fusion Research 1986 (IAEA, Vienna, 1987), Vol. 2, paper IAEA-CN-47/C-II-1.

16. Smith, G.R., Nevins, W.M., Cohen, R.H., Kritz, A.H., Bull. Am. Phys. Soc. **31** (1986) 1516.

17. Shkarofsky, I.P., J. Plasma Phys. **35** (1986) 319.

18. Akhiezer, A.I., Akhiezer, I.A., Polovin, R.V., Sitenko, A.G., and Stepanov, K.N., *Plasma Dynamics,* Vol. I (Pergamon, Oxford, 1975).
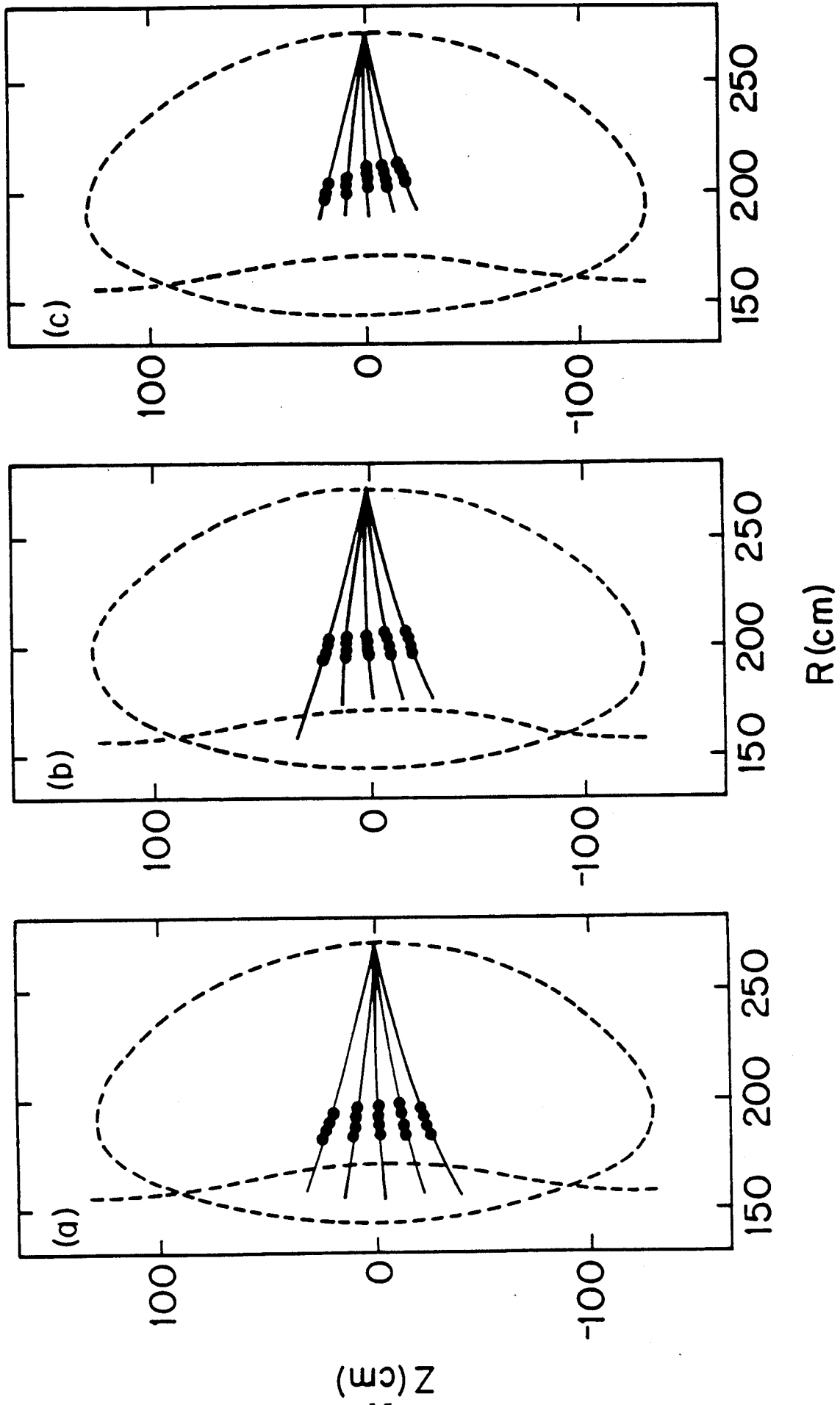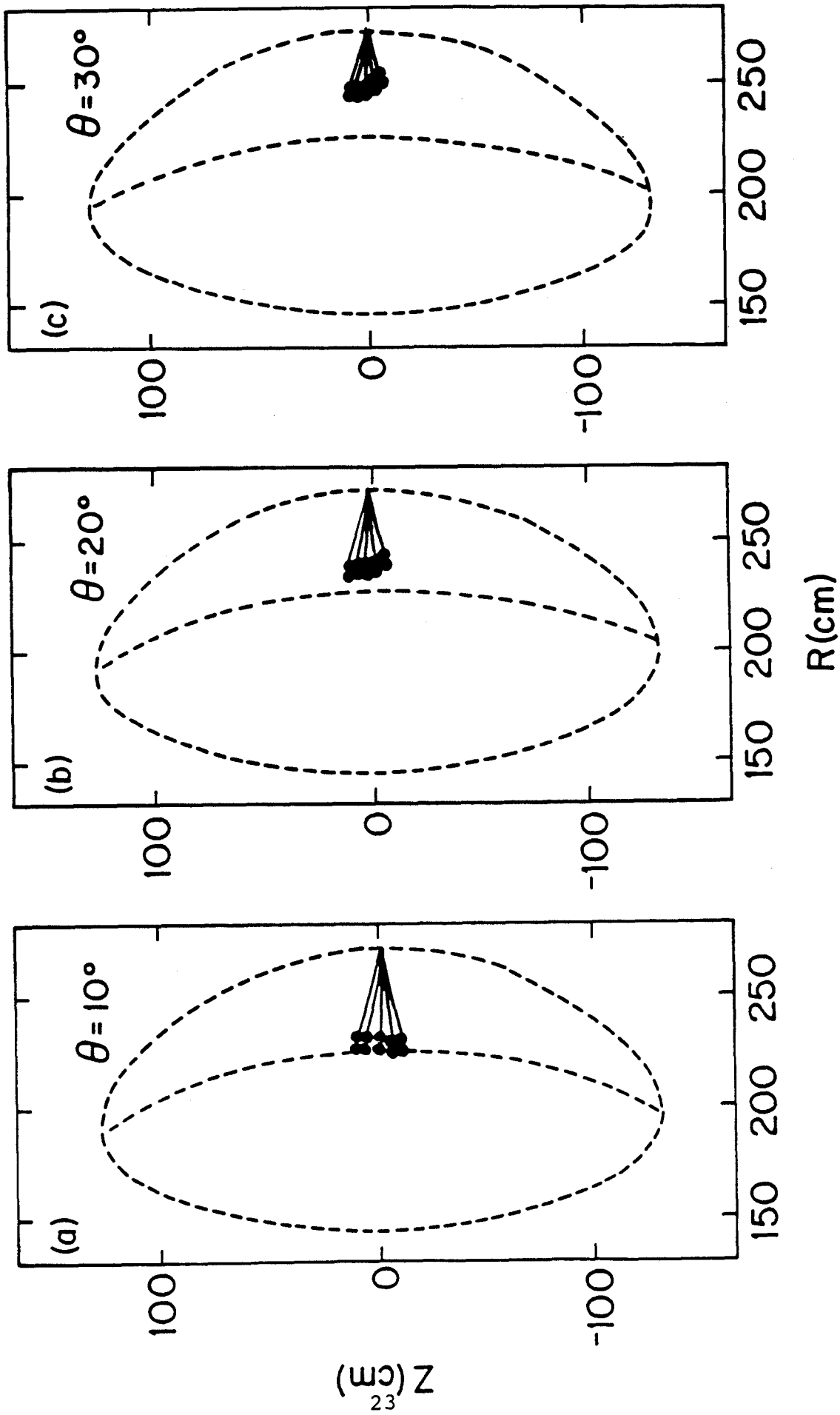
Figure 1

15

$\theta = 10°$ (a)

$\theta = 20°$ (b)

$\theta = 30°$ (c)

R(cm)

Z(cm)

23

Figure 9